

Effect of Ni on Microstructure and Mechanical Properties of CrMnFeCoNi High Entropy Alloy

Suresh Koppoju¹  · Satya Prasad Konduri¹ · Prashanthi Chalavadi¹ · Srinivasa Rao Bonta^{1,2} · Ramakrishna Mantripragada¹

Received: 13 August 2019 / Accepted: 23 October 2019 / Published online: 7 November 2019
© The Indian Institute of Metals - IIM 2019

Abstract The effect of Ni content on microstructure and mechanical properties of the CrMnFeCoNi high entropy alloy (HEA) has been studied. The Ni content varied from 0 to 20 at% in the composition $(\text{CrMnFeMn})_{100-x}\text{Ni}_x$, where $x = 0, 2.5, 5, 10, 15,$ and 20 at%. The alloys were synthesized by vacuum arc melting and the microstructure as well as hardness of the as-cast alloys were studied. Alloys with low Ni content ($x \leq 2.5\%$) consists of a two-phase microstructure of dendritic and inter-dendritic regions with fcc (matrix) and tetragonal (sigma) crystal structure, respectively. When the Ni content is 5 at%, two-phase structure with fcc (matrix) and bcc (secondary phase) is observed, with the addition of Mn-rich inclusions that are present in the entire matrix. Alloys with higher Ni content ($x \geq 10, \text{at}\%$) exhibit a single phase of fcc structure. Hardness of the HEAs decreases from 320 to 120 Hv with increase in Ni content, and the high hardness of these alloys with low Ni content is due to the mixture of both fcc and hard tetragonal (sigma) phases.

Keywords High entropy alloy · Microstructure · Transmission electron microscopy

1 Introduction

Conventional alloys consisting of a principal element with various concentrations of minor elements have been studied extensively for structural and functional applications in the last two centuries. Recently a new alloy design concept has emerged where there are two or more principal elements in equi- or near-equiatomic compositions resulting in a single-phase alloy due to the exceptional high configurational entropy (lowest Gibbs free energy) [1, 2]. This class of new alloys has been named as high entropy alloys or multicomponent alloys [1, 2]. Most of the reported single-phase HEAs have the face-centered cubic (fcc) or body-centered cubic (bcc) structure, with the rare occurrence of hexagonal close-packed (hcp) phases [3–5]. One of the earliest reported HEAs is the quinary CrMnFeCoNi alloy (Cantor alloy) which is a single phase with fcc structure [2]. The alloy continues to be investigated to understand the structure–property relations as a model for HEAs [6]. The alloy also possesses outstanding mechanical properties at room temperature as well as cryogenic temperatures (-196 °C) owing to an additional deformation mechanism, namely nano-twinning [6–8].

Another school of thought is that, non-equiatomic HEAs may exhibit better properties than equiatomic alloys for wider applications [9]. This argument has been supported by theoretical calculations which predict that non-equiatomic quinary Cr–Mn–Fe–Co–Ni HEA will be stronger than the equiatomic CrMnFeCoNi alloy and that the yield strength of the former is higher by 100 MPa [10]. Li et al. [11] have reported the formation of non-equiatomic two-

Electronic supplementary material The online version of this article (<https://doi.org/10.1007/s12666-019-01838-2>) contains supplementary material, which is available to authorized users.

✉ Suresh Koppoju
sureshkoppoju@arci.res.in

¹ Centre for Materials and Characterization and Testing (CMCT), International Advanced Research Centre for Powder Metallurgy and New Materials (ARCI), Balapur PO, Hyderabad, Telangana 500 005, India

² Department of Metallurgy, National Institute of Technology-Warangal, Warangal, Telangana 506004, India

phase $\text{Fe}_{80-x}\text{Mn}_x\text{Co}_{10}\text{Cr}_{10}$ HEA through transformation-induced plasticity (TRIP) mechanism, which yields an excellent combination of strength ductility. Fang et al. reported a non-equiatom quaternary $\text{Co}_{35}\text{Cr}_{25}\text{Fe}_{40-x}\text{Ni}_x$ ($x = 0-15$) HEA that possesses an excellent combination of the tensile strength of a maximum of 1000 MPa and elongation of 35%, owing to solid solution strengthening augmented with TRIP effect [12]. Li et al. [13] have used an ab initio-assisted alloy design approach to screen for new HEAs and found that the non-equiatom quinary $\text{Cr}_{20}\text{Mn}_{20}\text{Fe}_{36}\text{Co}_{20}\text{Ni}_6$ compound exhibits higher tensile strength (more than 150 MPa) and higher strain-hardening ability compared to the corresponding equiatom CrMnFeCoNi alloy owing to the TRIP effect. The non-equiatom quinary $\text{Cr}_{20}\text{Mn}_{20}\text{Fe}_{36}\text{Co}_{20}\text{Ni}_6$ HEA possesses two-phase structure, with the volume fraction of the fcc and hcp phases being 94% and 6%, respectively. Choi et al. [10] have reported that by reducing or removing Co and Ni one by one from quinary CrMnFeCoNi HEA, the alloy becomes unstable, and hence it is essential to have Co and Ni in the alloy. However, since Co and Ni are expensive, reduced usage of these elements will be greatly beneficial from a commercial point of view. If one is able to synthesize a HEA with lower content of Co or Ni in quinary Cr-Mn-Fe-Co-Ni with comparable or superior mechanical properties, it can be useful for a wide range of applications. Zhu et al. [14] studied the structural stability of CrMnFeCoNi HEA with Co and found that the HEAs are not stable at low concentrations of Co. Therefore, it is necessary to investigate the effect of Ni on the evolution of microstructure, constituent phases and mechanical properties of quinary CrMnFeCoNi HEA. In the present study, development of the microstructure and mechanical properties of the as-cast $(\text{CrMnFeCo})_{1-x}\text{Ni}_x$ HEA, where $x = 0, 2.5, 5, 10, 15$ and 20 at%, is reported. This study also reports microstructural data which will be an input for computational studies to calculate important intrinsic parameters such as elastic constant and critical resolved shear stress (CRSS) parameters for the design of new HEAs.

2 Experimental

Alloys with composition of $(\text{CrMnFeCo})_{1-x}\text{Ni}_x$, where $x = 0.0, 2.5, 5, 10, 15$ and 20 at%, were prepared using the vacuum arc-melting technique. A sample of 10 g of each alloy composition was prepared using high-purity (99.9%) elements. Before melting of the sample, the arc-melting chamber was purged with high-purity Ar gas thrice and to further remove trace oxygen, Ti metal getter was melted. In order to ensure chemical homogeneity, the button that formed after the first melting was re-melted by flipping it

up-side down after each melt for five times. To obtain the desirable composition of the melted alloy, 10% of Mn was additionally added to the sample since Mn has a high vapor pressure of 7.54 mBar at 1400 °C [15]. The nomenclature of each of the compositions is as follows: $(\text{CrMnFeCo})_{100}$ ($x = 0$, at%) as N0, $(\text{CrMnFeCo})_{97.5}\text{Ni}_{2.5}$ ($x = 2.5$ at%) as N2.5, $(\text{CrMnFeCo})_{95}\text{Ni}_5$ ($x = 5$ at%) as N5, $(\text{CrMnFeCo})_{90}\text{Ni}_{10}$ ($x = 10$ at%) as N10, $(\text{CrMnFeCo})_{85}\text{Ni}_{15}$ ($x = 15$ at%) as N15, and $(\text{CrMnFeCo})_{80}\text{Ni}_{20}$ ($x = 20$ at%) as N20. The as-cast buttons were considered for microstructural studies and mechanical property evaluation.

Powder X-ray diffraction was carried out using a Bruker D8 Advance unit with $\text{Cu}_{k\alpha}$ radiation for phase identification. Microstructural studies were carried out by optical microscopy (Olympus, Model: DSX510), scanning electron microscopy (Zeiss FE-SEM GEMINI500) and transmission electron microscopy (FEI-G2, 200 kV) with energy-dispersive spectroscopy (EDAX-TSL). Specimens for TEM studies were prepared by the twin jet electro-polishing technique using 15% perchloric acid with methanol. Bulk hardness was measured on samples with a load of 1 kg using a Vickers macro-hardness tester (LECO, Model: LV-700AT). An average value of the hardness obtained from more than ten indentations that were made on the samples has been reported in this manuscript. JEMS electron microscopy simulation software has been used to analyze the selected area electron diffraction (SAED) patterns, especially to analyze the tetragonal phase of Cr-Mn-Fe-Co-(Ni) in the N0 and N2.5 compositions.

3 Results

XRD patterns of as-cast $(\text{CrMnFeCo})_{100-x}\text{Ni}_x$ HEAs with Ni content from 0 to 20 at% are shown in Fig. 1. It can be observed that the diffracted intensities of the patterns are not as expected indicating that the as-cast microstructure possesses crystallographic texture that develops during the solidification. The XRD patterns of N0 and N2.5 show the presence of two-phase structure, which is identified as matrix phase with face-centered cubic (fcc) structure with space group (SG) of fm-3 m and the second phase with tetragonal structure SG of P42/mnm [16]. The XRD patterns of N0 and N2.5 agree with the reported XRD profile of as-cast CoCrFeMn HEA that has the presence of a tetragonal phase in addition to the matrix fcc phase [17]. The XRD profile of the N5 composition mainly exhibits the fcc phase with an additional peak at 2θ of 46.86° , corresponding to the Miller indices of the (110) planes of body-centered cubic phase with inter-planar spacing (d) of 1.972 \AA . The XRD patterns of N10, N15, and N20 show a single phase with fcc structure. Lattice parameters of the

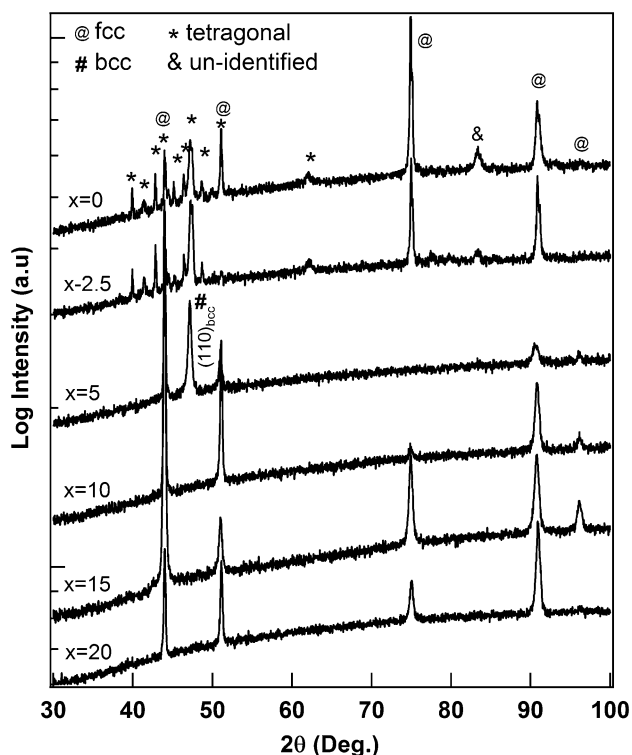


Fig. 1 Superimposed XRD patterns of the as-cast $(\text{CrMnFeCo})_{1-x}\text{Ni}_x$ HEA with Ni content

fcc, tetragonal and bcc phases with Ni content have been calculated and are provided in Table 1. The lattice parameter of the fcc phase slightly decreases with the increase in the Ni content in $(\text{CrMnFeCo})_{100-x}\text{Ni}_x$ (Table 1) owing to the smaller atomic radius of the Ni. The lattice parameter ($a = 3.589(3) \text{ \AA}$) of the fcc phase of the N20 HEA is comparable to the value in earlier reports [18],

and the lattice parameters ($a = 8.773(7) \text{ \AA}$ and $4.594(5) \text{ \AA}$) of the tetragonal phase of the N0 HEA are also in good agreement with Ref. [19].

The as-cast microstructure of the $(\text{CrMnFeCo})_{100-x}\text{Ni}_x$ HEAs with Ni content is shown in Fig. 2. The N0 and N2.5 HEAs exhibit the two-phase microstructure of dendritic and inter-dendritic regions (Fig. 2a, b), whereas N5 HEA (Fig. 2c) possesses evenly distributed islands in the matrix phase. No trace of bcc phase (Fig. 2c) is observed in the N5 HEA as the signature of the diffracted peak observed from the XRD pattern (Fig. 1). The other alloys also consist of such islands with reduced size and number. The volume fraction of the second phase (dark contrast), which includes inclusions, decreases with Ni content (Fig. S1). Presence of the secondary (tetragonal) phase is more than 23% in the N0 and N2.5 HEAs while the second phase occurring in islands rapidly decreases to less than 5% in the N5 HEA with slight increase in Ni content from $x = 2.5$ –5 at%, and further, the phase fraction of islands (Mn-rich particles) decreases to less than 1% in the N15 and N20 HEAs [14].

Transmission electron microscope bright field (BF) image of the N0 HEA is shown in Fig. 3. It can be observed from Fig. 3a that the region of slight dark contrast corresponds to the matrix phase, whereas bright region corresponds to inter-dendritic secondary phase (P2). The chemical composition, obtained using TEM-EDS (Fig. 3b) of the matrix phase (P1), is the nearly equiatomic composition of CrMnFeCo alloy (Table 2). The secondary phase also consists of all the principal Cr, Mn, Fe, and Co elements in major fraction, but is enriched with Cr and slightly depleted in Co as compared to the matrix composition (Table 2). Crystal structure of the matrix (P1) and the secondary phase (P2) have been independently determined

Table 1 Lattice parameters of the various phases in the as-cast $(\text{CrMnFeCo})_{1-x}\text{Ni}_x$ HEA with Ni content

S. no.	Alloy	Technique	Lattice parameter (\AA)			
			a (fcc)	a (tetra.)	c (tetra.)	a (bcc)
1	$x = 0$	XRD	3.597 (5)	8.773 (5)	4.594 (4)	–
		TEM	3.65 (3)	8.86 (7)	4.56 (3)	–
2	$x = 2.5$	XRD	3.595 (7)	8.790 (2)	4.538 (3)	–
		TEM	3.65 (2)	8.82 (2)	4.52 (4)	–
3	$x = 5$	XRD	3.596 (6)	–	–	2.739
		TEM	3.67 (2)	–	–	–
4	$x = 10$	XRD	3.592 (4)	–	–	–
		TEM	3.67 (3)	–	–	–
5	$x = 15$	XRD	3.594 (4)	–	–	–
		TEM	3.64 (4)	–	–	–
6	$x = 20$	XRD	3.589 (3)	–	–	–
		TEM	3.62 (2)	–	–	–

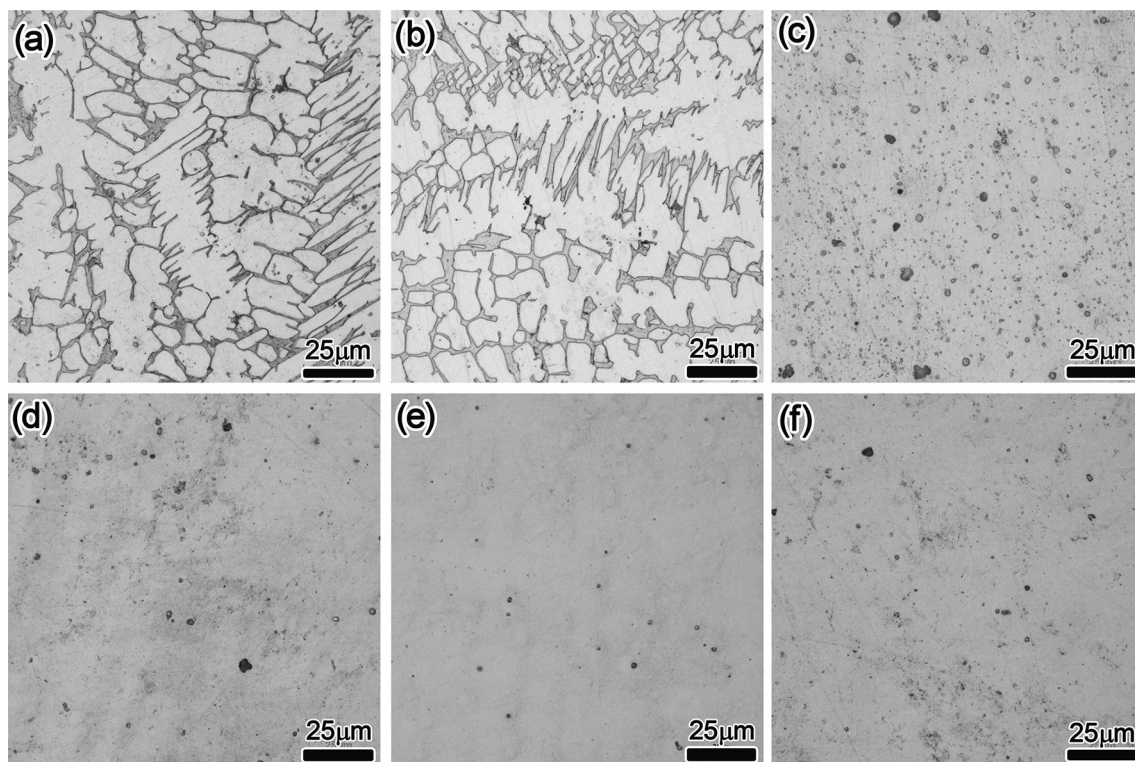


Fig. 2 Optical micrographs of the as-cast $(\text{CrMnFeCo})_{1-x}\text{Ni}_x$ HEA with Ni content, **a** $x = 0$, **b** $x = 2.5$, **c** $x = 5$, **d** $x = 10$, **e** $x = 15$ and **f** $x = 20$ at%

using selected area electron diffraction (SAED) (Figs. 3c–f) with a minimum of two diffraction patterns from different zone axes. The SAED patterns obtained from the matrix phase, using zone axes of [001] and [011] (Fig. 3c, d), confirm that the phase has face-centered cubic (fcc) structure with a lattice parameter of 3.65 Å, which is similar to lattice parameter obtained by XRD [18]. Analysis of three diffraction patterns obtained (Fig. 3e–g) using zone axes of [001], [110] and [111] from the secondary phase with support of simulated electron diffracted pattern (Fig. 3h) using JEMS software confirms further that the phase (P2) is tetragonal with lattice parameters of $a = 8.86$ Å and $c = 4.56$ Å, which is in good agreement with the values obtained from XRD studies. Similarly, the microstructure of the N2.5 alloy also consists of two phases (Fig. S2) with matrix phase being fcc and the secondary inter-dendritic phase being tetragonal. Lattice parameters of these phases are similar to the N0 HEA (Table 1). A small fraction of Ni is present in the tetragonal phase (Table 2). Detailed investigation of the microstructure (TEM-BF) (Fig. 4) of the N5 alloy reveals that it has a bcc structure (Fig. 4a), in addition to the matrix fcc phase. The second phase is confirmed to have a bcc crystal structure with SAED patterns that are obtained from the zone axes of [001], [011] and [111] (Fig. 4b–d). The matrix is confirmed to be fcc by SAED pattern obtained from the [011] zone

axis (Fig. 4e). The presence of bcc phase in the N5 HEA is further confirmed with the TEM investigation, as the XRD profile of the N5 HEA has only one diffracted peak at 2θ of 46.86° from the bcc phase. The chemical composition of the bcc phase also contains all the principal elements (Fig. 4f), and it is enriched with Cr, and has a presence of Ni around 2 at% (Table 2). The presence of the Mn-rich particles in the N5 HEA is also sometimes observed as shown in Fig. S3 along with EDS profile that is obtained from the particle. The estimated average lattice parameters of the N5 HEA using the SAED patterns of the fcc and the bcc phases are 3.67 Å and 2.82 Å, respectively. Alloys with Ni ≥ 10 at% show a single phase with fcc structure, which is confirmed from both the XRD and TEM studies. The microstructure of the alloys with N10 and N15 (Fig. S4) and N20 (Fig. 5) exhibits only the presence of single phase of fcc structure, which is in good agreement with XRD studies (Fig. 1). The phases present in the alloys and their lattice parameters obtained from SAED are also provided in Table 1.

The Vickers hardness of a $(\text{CrMnFeCo})_{100-x}\text{Ni}_x$ HEA with Ni content is shown in Fig. 6. The alloys N0 and N2.5 exhibit high hardness of above 310 HV. With the increase in Ni content, hardness rapidly decreases for the N5 alloy to about 160 HV and the other alloys with high Ni content exhibit hardness close to 120 HV. The hardness of N20 is very close to that reported in the literature [20].

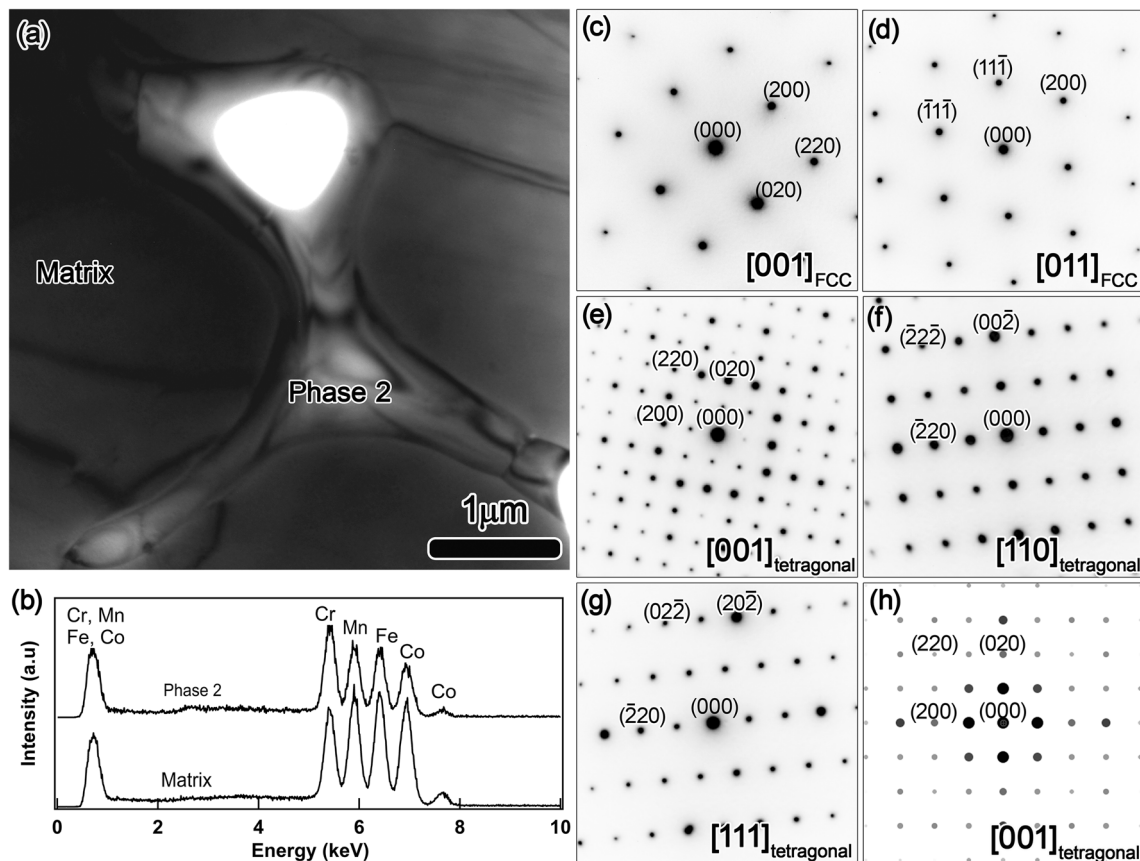


Fig. 3 **a** Bright field image of the as-cast quaternary $(\text{CrMnFeCo})_{1-x}\text{Ni}_x$ HEA with $x = 0$ at% shows the presence of two-phase structure (matrix and phase 2), **b** EDS spectra from matrix and phase 2, **c–g** selected area electron diffraction (SAED) patterns from matrix and phase 2 with different zone axes. **c**, **d** SAED patterns from matrix with zone axes of $[001]_{\text{FCC}}$ and $[011]_{\text{FCC}}$, and **e**, **f** SAED patterns from phase 2 with zone axes of $[001]_{\text{tetragonal}}$, $[011]_{\text{tetragonal}}$ and $[111]_{\text{tetragonal}}$, and **(h)** simulated SAD pattern with zone axis of $[001]_{\text{tetragonal}}$ phase

4 Discussion

Microstructural studies reveal the presence of two-phase structure in N0, N2.5, and N5 HEAs, whereas the other HEAs exhibit only single phase with the fcc structure. However, these alloys contain Mn-rich inclusions (may be sulfides or oxides), which are commonly present in Mn-containing alloys [21]. The N0 and N2.5 HEAs have a matrix which is dendritic with the fcc structure, and a second inter-dendritic tetragonal phase, while the N5 HEA has the second phase that is bcc rather than tetragonal, in addition to the matrix fcc phase. Therefore, with the increase in Ni content in $(\text{CrMnFeCo})_{100-x}\text{Ni}_x$ HEA, the second phase initially ($x = 0–5$ at%) has the tetragonal structure which transforms to bcc phase. For the HEA with $x \geq 10$ at%, the second phase disappears altogether, with only the matrix fcc remaining.

To understand the phase evolution in as-cast $(\text{CrMnFeCo})_{100-x}\text{Ni}_x$ HEAs, pseudobinary phase diagram with the Ni composition from 0 to 20 at% has been calculated using Thermo-cal database as shown in Fig. 7. The

predicted phases at room temperature are fcc, bcc and sigma, which exist throughout the calculated composition, but these phases and their fractions are not exactly corroborated by the experimental data due to the limitations of the input parameters of the database for HEA compositions. Although the calculated phase fractions are not in good agreement with the experimental data, the calculated phase diagram provides an insight into the possible phases which have been experimentally observed in this work. The sigma (tetragonal) phase is present in the N0 and N2.5 compositions of the matrix fcc phase, and with further increase in Ni to 5 at%, the sigma phase disappears, with the appearance of the bcc phase. The chemical composition of both the sigma and the bcc phases is nearly similar within the variation of a few at% (Table 2). From the Fe–Cr phase diagram [22, 23], it is well known that the sigma phase ($\text{Fe}_{50}\text{Cr}_{50}$) is bcc [23], and when the Fe content is slightly increased by 1%, ($\text{Fe}_{51}\text{Cr}_{49}$, at%), it transforms to the tetragonal crystal structure [24]. In the case of multi-component Cr–Mn–Fe–Co–Ni alloy, the tetragonal sigma phase is enriched with Cr by around ~ 35 at%, as is seen

Table 2 Composition (at%) of the various phases in the as-cast (CrMnFeCo)_{1-x}Ni_x HEA with Ni content

S. no.	Alloy	Phases	Composition (at%)				
			Cr	Mn	Fe	Co	Ni
1	$x = 0$	Alloy	24.78	25.61	24.68	24.91	0
		Matrix	24.30	24.10	25.70	26.00	0
		Secondary (tetragonal)	35.00	22.70	23.20	19.20	0
2	$x = 2.5$	Alloy	25.04	24.08	23.46	23.99	2.23
		Matrix	23.68	23.22	23.98	26.2	2.88
		Secondary (tetragonal)	35.48	21.54	22.12	19.68	1.2
3	$x = 5$	Alloy	23.52	24.12	24.17	23.63	4.56
		Matrix	21.19	22.61	24.98	23.42	4.80
		Secondary (bcc)	37.9	22.0	20.65	17.4	2.1
		Mn-rich particles	8.28	85.90	2.45	2.51	0.86
4	$x = 10$	Alloy	22.83	23.06	22.15	22.33	9.63
		Mn–Cr rich particles	49.97	44.58	4.86	4.41	2.20
5	$x = 15$	Alloy	21.23	22.20	21.41	20.34	14.82
		Mn-rich particles	17.60	60.24	8.49	8.20	5.52
6	$x = 20$	Alloy	21.17	19.30	20.65	19.59	19.20

from previous report [25]. In the present study, the chemical composition of the sigma phase is similar to published values except Ni content [25] and the bcc phase has a slightly higher content of Cr than the sigma phase. We propose that the transformation of the bcc phase from tetragonal sigma phase is not due to the Cr content alone, but also due to the matrix phase environment. Further increase in Ni ($x \geq 10$) leads to the formation of a single fcc structure, although Mn-rich inclusions are still present in these alloys with low fraction.

In addition to the support obtained from the pseudo-binary phase diagram inputs from the widely used semi-empirical entropy parameters such as entropy of mixing (ΔS_{mix}), enthalpy of mixing (ΔH_{mix}), the atomic size difference (δ), and the Zhang parameter [scaled ratio of (ΔS_{mix}) to (ΔH_{mix})] can also be used to study the evolution of phases with Ni content in the (CrMnFeCo)_{100-x}Ni_x HEA. These parameters have been calculated using the following relations [26–31].

$$\Delta S_{\text{mix}} = -R \sum_{i=1}^n (c_i \ln c_i) \quad (1)$$

where R , c and n represent the universal gas constant, the atomic percentage at%, the number of the elemental components, respectively.

$$\Delta H_{\text{mix}} = \sum_{i=1}^n 4\Delta H_{ij}^{\text{mix}} c_i c_{j,i=j} \quad (2)$$

where $\Delta H_{ij}^{\text{mix}}$ is the enthalpy of mixing of i th and j th elemental components,

$$\delta = \sqrt{\sum_{i=1}^n c_i \left(1 - \frac{r_i}{\sum_{i=1}^n (c_i r_i)}\right)^2} \quad (3)$$

where r_i is the atomic radius of the i th constituent element,

$$\Omega = \frac{\Delta S_{\text{mix}} \sum_{i=1}^n c_i (T_m)_i}{|\Delta H_{\text{mix}}|} \quad (4)$$

where $(T_m)_i$ is the melting point of the i th constituent element.

According to Guo et al. [27], when the calculated entropy parameters of HEA fall within the ranges of $11 \leq \Delta S_{\text{mix}} \leq 19.5 \text{ JK}^{-1} \text{ mol}^{-1}$, $-22 \leq \Delta H_{\text{mix}} \leq 7 \text{ kJ mol}^{-1}$, $0 \leq \delta \leq 8.5\%$, and further, when $\Omega \geq 1.1$, the HEA is expected to form a solid solution. The favorability of formation of solid solution of the HEA increases with a higher value of the ΔS_{mix} , lowest (–ve) values of ΔH_{mix} , δ being close to zero, and $\Omega > 1.1$ [27]. The ΔS_{mix} , ΔH_{mix} , δ , and Ω parameters have been calculated for the (CrMnFeCo)_{100-x}Ni_x HEAs of the present study as a function of Ni content, and are shown in Fig. 8. The compositions of the HEAs used for the parameter calculations are obtained from SEM–EDS measurements (Table 2) while the required inputs to calculate the entropy parameters have been obtained from Ref. [27]. It can be observed from Fig. 8 that with an increase in Ni content for $x = 0$ –20 at%, the entropy of mixing (ΔS_{mix}) increases from 11.52 to 13.38 $\text{J mol}^{-1} \text{ K}^{-1}$ (Fig. 8a), whereas enthalpy of mixing (ΔH_{mix}) decreases from -2.29 to $-4.16 \text{ kJ mol}^{-1}$ (Fig. 8a). Similar to ΔH_{mix} , the atomic size difference (δ) and Zhang parameter (Ω) also decrease

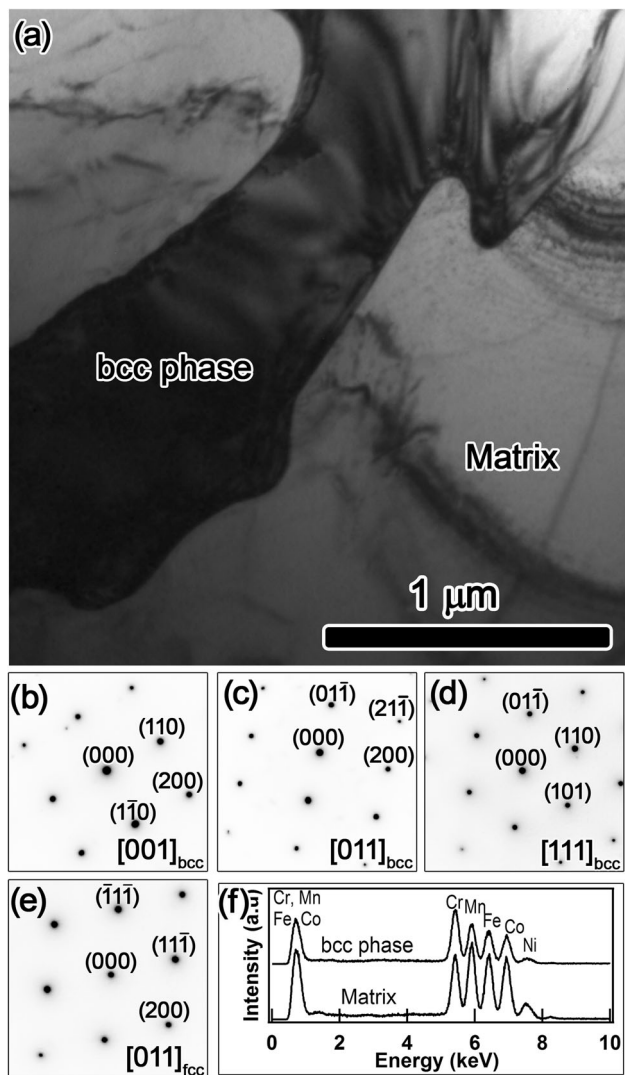


Fig. 4 a Bright field image of the as-cast quinary $(\text{CrMnFeCo})_{1-x}\text{Ni}_x$ HEA with $x = 5$ at% showing the presence of two-phase (matrix and bcc), b–e SAED patterns from the matrix and bcc phases with different zone axes. b–d SAED patterns from bcc phase with zone axes of $[001]_{\text{bcc}}$, $[011]_{\text{bcc}}$ and $[111]_{\text{bcc}}$, and e SAED patterns from the matrix with zone axis of $[011]_{\text{fcc}}$, and (f) EDS spectra from matrix and bcc phase

from 3.48 to 3.27, and 9.17–5.79, respectively (Fig. 8b). All these four entropy parameters thus satisfy the criteria to form a solid solution of the $(\text{CrMnFeCo})_{100-x}\text{Ni}_x$ HEAs with Ni content up to 20 at% as seen from the present study. However, microstructural studies reveal the presence of two phases with Ni content up to 5 at%, while alloys with Ni content $x \geq 10$ at% form a single phase, which is in the corroboration with the semi-empirical criteria of the higher value of ΔS_{mix} , lower value of ΔH_{mix} and the smaller value of δ .

The other important parameter is valance electron concentration (VEC) which predicts the formation of the

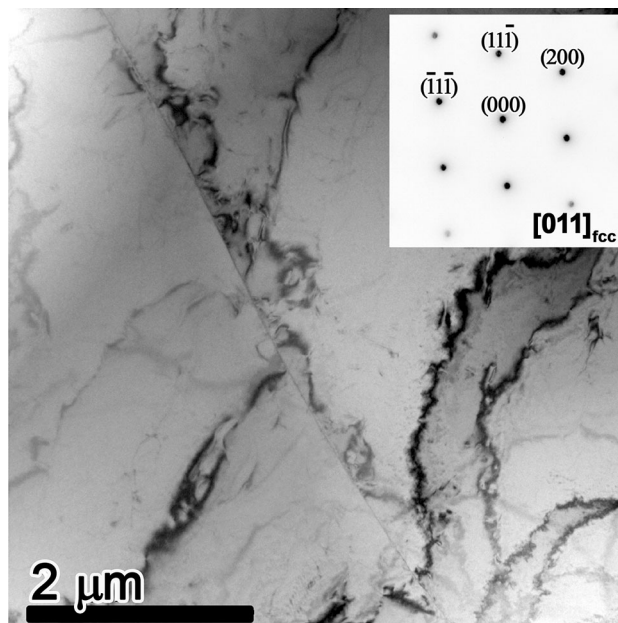


Fig. 5 Bright field image of the as-cast quinary the $(\text{CrMnFeCo})_{1-x}\text{Ni}_x$ HEA with $x = 20$ at%. Inset shows SAED patterns from the zone axis of $[011]_{\text{fcc}}$

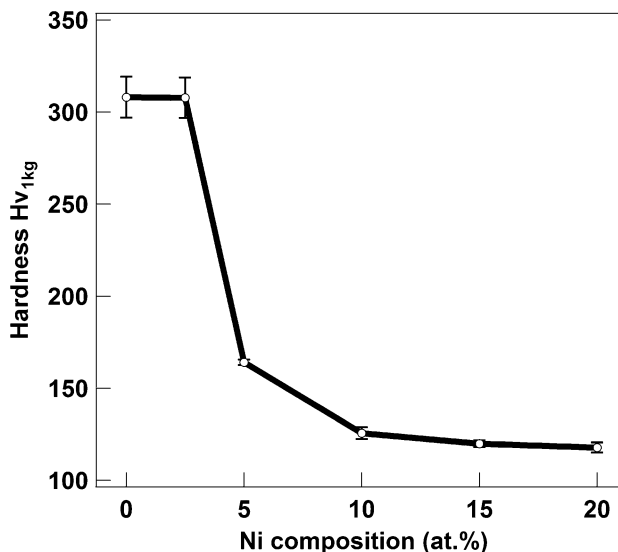


Fig. 6 Vickers hardness of the as-cast $(\text{CrMnFeCo})_{1-x}\text{Ni}_x$ HEA with Ni content

possible phase that may be formed and can be estimated using following relation

$$\text{VEC} = \sum_{i=1}^n c_i(\text{VEC})_i \tag{5}$$

where $(\text{VEC})_i$ is the VEC of the i th constituent element.

Guo et al. have proposed that when VEC is above 8, a single fcc phase will be formed and when VEC is below 6.8, single bcc phase is expected. When $6.8 < \text{VEC} < 8$,

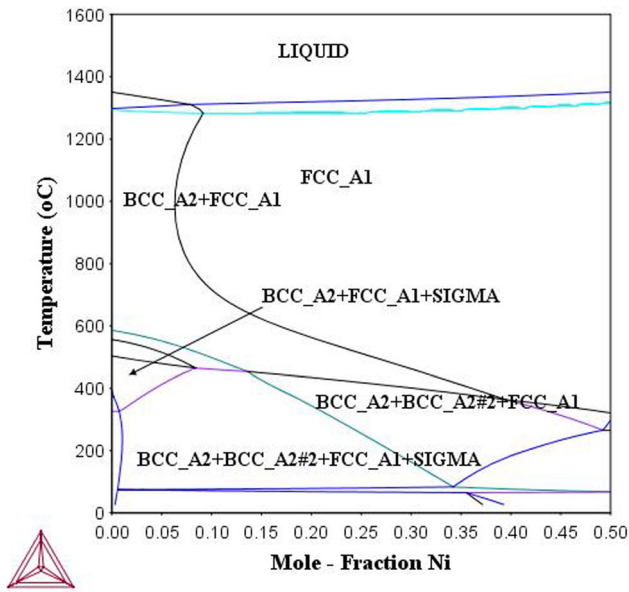


Fig. 7 Pseudo-binary phase diagram of the $(\text{CrMnFeCo})_{1-x}\text{Ni}_x$ HEA with Ni content

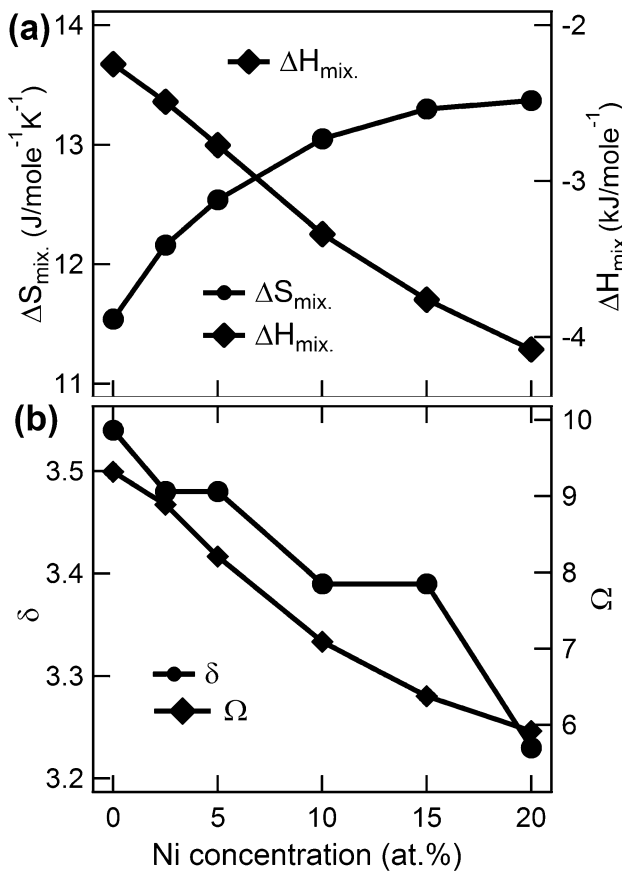


Fig. 8 ΔS_{mix} , ΔH_{mix} , δ , and Ω of the $(\text{CrMnFeCo})_{1-x}\text{Ni}_x$ HEA with Ni content

the formation of dual phase is expected with the fcc and the bcc crystal structures [27–29, 31]. Further, Tsai et al. [32] have proposed a modified criterion for VEC, stating that the HEAs with the VEC value between 6.8 and 7.8 have high propensity to form the tetragonal phase during casting or post-heat treatment process (aging). Figure 9 shows that the VEC of the $(\text{CrMnFeCo})_{100-x}\text{Ni}_x$ HEAs increases from 7.53 to 7.97 with the Ni content. According to the VEC values, this HEA should have a two-phase structure consisting of fcc and bcc phases. The N5 alloy only possesses dual phases of fcc and bcc which is in agreement with predictions of the VEC proposed by Guo et al. [27, 28]. The low Ni content N0 and N2.5 alloys possess the tetragonal (σ) phase instead of the bcc phase along with matrix fcc phase. To estimate the propensity for the formation of the tetragonal phase, and its volume fraction from the fcc matrix, Tasi et al. [32] proposed a parameter called paired sigma-forming element (PSFE) content in addition to the VEC. The PSFE is proposed based on the elements that are present in the alloy such as Cr and Mo which have the propensity to form binary sigma phases and tend to form binary sigma phases with Mn, Fe, and Co elements, these elements being named as sigma forming elements (SFEs) [32]. The fraction of the sigma phase is directly related to the availability of SFEs in the HEA that form an equiatomic binary sigma phase (for, example $\text{Fe}_{50}\text{Cr}_{50}$). The sigma phase only develops when PSFE content in the HEA is above a threshold value of more than 20%, though VEC of the HEA value falls in the range of 6.8–8 for the sigma-forming region [32].

The calculated PSFE content at% with Ni for the $(\text{CrMnFeCo})_{100-x}\text{Ni}_x$ HEAs is shown in Fig. 9, which decreases from 50 to 40 with the increase in Ni content from $x = 0$ to 20 at%. The PSFE content is higher than 40% in all alloys, and the VEC of the alloys also falls in the sigma-forming

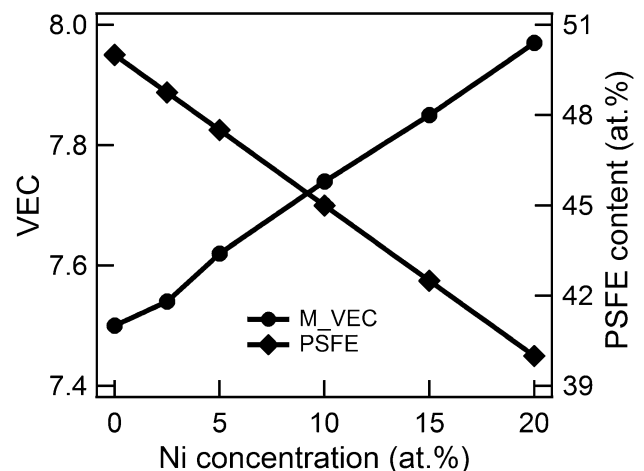


Fig. 9 VEC and PSFE content of the $(\text{CrMnFeCo})_{1-x}\text{Ni}_x$ HEA with Ni content

Table 3 The calculated δ , ΔH_{mix} , ΔS_{mix} , Ω , VEC parameters and PSFE content for the $(\text{CrMnFeCo})_{1-x}\text{Ni}_x$ HEA with Ni content

S. no.	Alloy	δ (%)	ΔH_{mix} (kJ mol ⁻¹)	ΔS_{mix} (Jmol ⁻¹ K ⁻¹)	Ω	VEC	PSFE content (at%)
1	$x = 0$	3.54	- 2.25	11.54	9.32	7.50	50
2	$x = 2.5$	3.48	- 2.49	12.16	8.89	7.54	48.75
3	$x = 5$	3.48	- 2.77	12.54	8.21	7.62	47.5
4	$x = 10$	3.39	- 3.34	13.05	7.09	7.74	45.0
5	$x = 15$	3.9	- 3.76	13.30	6.38	7.85	42.5
6	$x = 20$	3.23	- 4.08	13.37	5.92	7.97	40

range. Thus, the $(\text{CrMnFeCo})_{100-x}\text{Ni}_x$ HEAs should form the sigma phase with Ni content up to 20 at%. In the present study, only the N0 and N2.5 compositions contain the tetragonal (sigma) phase with fraction of more than 20%. Among all the alloys, only N0 and N2.5 conform to both the sigma-phase forming criteria [32, 33]. The other alloys, especially those with higher Ni content ($x \geq 10$), satisfy the criterion to form a single phase with fcc structure. We have experimentally verified that the HEA with the composition $\text{Co}_{20}\text{Cr}_{40}\text{Fe}_{20}\text{Ni}_{20}$ and PSFE of 80% only contains 5% of the sigma phase [32]. This indicates that higher PSFE and VEC are alone not enough to explain the development of sigma phase in HEAs with higher Ni content. In the HEA with higher content (nearly close to equiatomic) without sigma phase-forming elements such as Mo, V, Ti, etc., Ni suppresses mostly the formation of Cr-Fe (Co, Mn) sigma phase and promotes the formation of fcc structure during solidification. Secondly, when the Ni content increases to 20 at%, the configurational entropy of HEAs (Fig. 8a) also increases, which may suppress the formation of the sigma phase. This will be interesting to investigate if the sigma phase is formed in these alloys when they are subjected to a post-heat treatment between from 500 to 900 °C for several hours (Table 3).

The hardness of the low Ni content $(\text{CrMnFeCo})_{100-x}\text{Ni}_x$ HEAs, N0 and N2.5, is above 300 Hv and that of the higher Ni content alloys is about 120 HV. The hardness of the equiatomic CrMnFeCoNi ($x = 20$ at%) HEA, which is only due to solid solution hardening, is similar to that reported in the literature [20]. Higher hardness in N0 and N2.5 is a composite value of the matrix fcc and secondary tetragonal (sigma) phases. The sigma phase is a hard phase, with very high hardness. In the case of the N5 alloy, hardness is about 160 HV because of the presence of the bcc phase and Mn-rich islands in the alloy.

5 Conclusions

In the present study, the effect of Ni content on the microstructure and the mechanical properties of $(\text{CrMnFeCo})_{100-x}\text{Ni}_x$ HEAs ($x = 0, 2.5, 5, 10, 15,$ and 20 at%) has been investigated. The summary of the work is as follows:

1. The HEAs with varying Ni content have been prepared by vacuum arc-melting method, and the microstructure and mechanical properties of the as-cast alloys have been studied.
2. The HEAs with low Ni content ($x \leq 5$ at%) consist of two-phase microstructure, whereas high Ni content ($x \geq 10$) alloys possess a single phase. The alloy with low Ni content ($x = 0$ and 2.5 , at%) contains the matrix dendritic arm fcc phase and secondary interdendritic region tetragonal (sigma) phase, while the 5 at% HEA consists of secondary bcc phase with fcc as a matrix phase. The HEAs with $\text{Ni} \geq 10$ at% form as single phase with fcc structure. Mn-rich inclusions have also been found in the HEAs with Ni content above 5 at%. Their fraction rapidly reduces from 10 to 1% with increasing Ni content from 5 to 20 at%.
3. The tetragonal (sigma) phase transforms into the bcc phase when the Ni content increases from 0 to 5 at%. With further increase in Ni content ($x \geq 10$), the sigma phase disappears in the HEAs.
4. The evolution of microstructure of the HEA with Ni content has been interpreted with the support from pseudobinary phase diagram and semi-empirical entropy parameters, especially using paired sigma-forming element (PSFE) content used for sigma phase formation.
5. High hardness of above 300 Hv has been observed for the HEA with low Ni content ($x = 0$ and 2.5 at%) owing to the presence of hard sigma phase. The hardness of around 120 Hv, which has been observed in the alloy with higher Ni content ($x \geq 10$), is attributed to solid solution strengthening.

Acknowledgements Authors would like to acknowledge Dr. Ravi C Gundakaram for his help with the manuscript and Ms. K. Anjali for calculations of the entropy parameters.

References

1. Cantor B, Chang I T H, Knight P, and Vincent A J B, *Mater Sci Eng A* **375–377** (2004) 213.
2. Yeh J W, Chen S K, Lin S J, Gan J Y, Chin T S, Shun T T et al., *Adv Eng Mater* **6** (2004) 299.

3. Praveen S, Murty B S, and Kottada R S, *Mater Sci Eng A* **534** (2012) 83.
4. Zhuang Y X, Liu W J, Chen Z Y, Xue H D, and He J C, *Mater Sci Eng A* **556** (2012) 395.
5. Tsau C H, *Mater Sci Eng A* **501** (2009) 81.
6. Otto F, Dlouhy A, Somsen C, Bei H, Eggeler G, and George E P, *Acta Mater* **61** (2013) 5743.
7. Shi P J, Ren W L, Zheng T X, Ren Z M, Hou X L, Peng J C, Hu P F, Gao Y F, Zhong Y B, and Liaw P K, *Nat Commun* **10** (2019) 8.
8. Lee C, Song G, Gao M C, Feng R, Chen P, Brechtl J, Chen Y, An K, Guo W, Poplawsky J D, Li S, Samaei A T, Chen W, Hu A, Choo H, and Liaw P K, *Acta Mater* **160** (2018) 158.
9. Zhiming Li and Raabe D, *JOM* **69** (2017) 2099. <https://doi.org/10.1007/s11837-017-2540-2>.
10. Choi W M, Jo Y H, Sohn S S, Lee S, and Lee B-J, *NPJ Comput Mater* **4** (2018) 1. <https://doi.org/10.1038/s41524-017-0060-9>.
11. Li Z, Pradeep K G, Deng Y, Raabe D, and Tasan C C, *Nature* **534** (2016) 227.
12. Fang W, Chang R, Ji P, Zhang X, Liu B, Qu X, and Yin F, *Metals* **8** (2018) 369 <https://doi.org/10.3390/met8050369>.
13. Li Z, Kormann F, Grabowski B, Neugebauer J, and Raabe D, *Acta Mater* **136** (2017) 262.
14. Zhu Z G, Ma K H, Yang X, and Shek C H, *J Alloys Compd* **695** (2017) 2945.
15. Yaws C L, *Safety and Health Related Properties for Organic and Inorganic Chemicals*, McGrahill Publication, New York (1999) p 182.
16. Shahmir H, He J, Lu Z, Kawasaki M, and Langdon T G, *Mater Sci Eng A* **676** (2016) 294.
17. Singh P, Marshal A, Smirnov A V, Sharma A, Balasubramanian G, Pradeep K G, and Johnson D D, *Phys Rev Mater* **3** (2019) 075002. <https://doi.org/10.1103/PhysRevMaterials.3.07500>.
18. Laplanche G, Gadaud P, Horst O, Otto F, Eggeler G, and George E P, *J Alloys Compd* **623** (2015) 348. <https://doi.org/10.1016/j.jallcom.2014.11.061>.
19. Cho K, Fujioka Y, Nagase T, and Yasuda H Y, *Mater Sci Eng A* **735** (2018) 191.
20. Salishchev G A, Tikhonovsky M A, Shaysultanov D G, Stepanov N D, Kuznetsov A V, Kolodiy I V, Tortika A S, and Senkov O N, *J Alloys Compd* **591** (2014) 11.
21. Gludovatz B, Hohenwarter A, Catoor D, Chang E H, George E P, and Ritchie R O, *Science* **345** (2014), 1153.
22. Kubaschewski O, *Phase Diagrams of Binary FeBased Systems*, Springer, Berlin (1982).
23. Turchi P E A, Reinhard L, and Stocks G M, *Phys Rev B Condens Matter Mater Phys* **50** (1994) 15542.
24. Yakel H L, *Acta Cryst Sec B Struct Sci* **39** (1983) 20.
25. Stepanov N D, Shaysultanov D G, Salishchev G A, Tikhonovsky M A, Oleynik E E, Tortika A S, and Senkov O N, *J Alloys Compd*, **628** (2015) 170.
26. Zhang Y, Zuo T T, Tang Z, Gao M C, Dahmen K A, Liaw P K, and Lu Z P, *Prog. Mater Sci* **61** (2011) 1.
27. Guo S and Liu C T, *Prog Nat Sci Mater Int* **21** (2011), 433.
28. Guo S, Ng C, Lu J, and Liu C T, *J Appl Phys* **109** (2011) 645.
29. Yang X and Zhang Y, *Mater Chem Phys* **132** (2012) 233.
30. Guo S, Hu Q, Ng C, and Liu C T, *Intermetallics* **41** (2013) 96.
31. Murty B S, Yeh J W, and Ranganathan S, *High Entropy Alloys*, Elsevier, London (2014).
32. Tsai M H, Tsai K Y, Tsai C W, Lee C, Juan C C, and Yeh J W, *Mater Res Lett* **1** (2013) 207.
33. Tsai M-H, Chang K-C, Li J-H, Tsai R-C, and Cheng A-H, *Mater Res Lett* **4** (2016) 90. <https://doi.org/10.1080/21663831.2015.1121168>.

Publisher's Note Springer Nature remains neutral with regard to jurisdictional claims in published maps and institutional affiliations.